ACS Catalysis

Research Article

pubs.acs.org/acscatalysis

Achieving High Electrocatalytic Efficiency on Copper: A Low-Cost Alternative to Platinum for Hydrogen Generation in Water

Jian Zhao,[†,‡,§,∥] Phong D. Tran,[*,†,§] Yang Chen,[†,§] Joachim S. C. Loo,[*,‡,§] James Barber,[§,⊥] and Zhichuan J. Xu[*,†,‡,§,∥]

[†]Energy Research Institute, [‡]School of Materials Science & Engineering, and [§]Solar Fuel Laboratory, Nanyang Technological University, 639798 Singapore

[∥]Singapore−Berkeley Research Initiative for Sustainable Energy, 1 Create Way, 138602 Singapore

[⊥]Department of Life Sciences, Imperial College London, London SW7 2AZ, U.K.

Supporting Information

ABSTRACT: A phosphate mediated (photo)electro-reduction process has been developed to activate cuprous oxide (Cu_2O) to copper−cuprous oxide (Cu/Cu_2O) for high efficient hydrogen evolution reaction (HER) in water at neutral pH. The activated copper-based electrode can efficiently catalyze HER with an impressive onset potential of −30 mV vs reversible hydrogen electrode (RHE), low Tafel slope of 60−80 mV·decade^{-1} and exchange current density j_0 of 3.0×10^{-5} A·cm^{-2}. This represents the first highly active copper-based electrocatalyst that could be used as a low-cost alternative to Pt for water electrolysis.

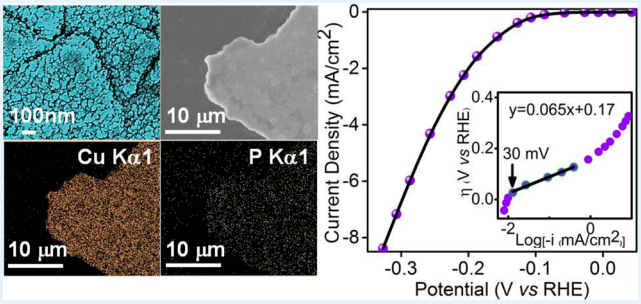

KEYWORDS: *copper electrode, cuprous oxide, phosphate, electrocatalysis, hydrogen evolution*

The urgent need for clean and renewable energy has stimulated considerable interest in developing solar hydrogen technologies, either by combining photovoltaics with water electrolyzers or by constructing photoelectochemical cells (PEC). In both cases highly efficient electrodes/catalysts are required to achieve high efficiencies of energy conversion to hydrogen. Electrolyzers and PEC systems consist of two electrodes: anode where the oxygen evolving reaction (OER) occurs and cathode where the hydrogen evolution reaction (HER) is achieved.[1−4] For the best systems the electrodes/catalysts are required to work in aqueous solutions at neutral or near-to-neutral pH with a small overpotential requirement, high catalytic rate (high exchange current density), and low Tafel slope. Moreover, for a cost-effective large scale technology, these systems should be made of components of earth-abundant and nontoxic elements. Unfortunately, these desirable criteria are difficult to achieve. For example, Pt shows the best performance for HER, but its high cost and nonabundance hinders its application for the development of scalable solar hydrogen technologies.

Over the past decade, significant advances have been achieved in designing efficient alternatives to Pt for HER based on first-row transition metals such as iron, cobalt, and nickel.[5−15] Besides these earth-abundant elements, copper is an attractive low cost metal and relatively less harmful to the environment compared with elements like cobalt and nickel. However, catalytic water splitting with copper-based electrocatalysts has not been well explored. It is only recently that a handful of molecular copper complexes have been shown to electrocatalyze OER.[16−19] Regarding HER, for a long time, copper had been considered to be an ineffective catalyst both in acidic and basic solution requiring a high overpotential of ca. 250−300 mV for hydrogen generation.[20−24] Recently, Sun et al. reported the very first copper(II) complex as a molecular catalyst for the H_2 from water which requires however a huge overpotential of 500 mV for functioning.[25]

In this paper, we report for the first time a highly active copper-based electrode for hydrogen generation from water at neutral pHs. This copper catalyst was prepared by a (photo)electrochemical reduction of Cu_2O in phosphate or carbonate buffer solution. The activated Cu/Cu_2O electrode catalyzes the HER in phosphate or carbonate solution with a very low overpotential of 30−50 mV vs reversible hydrogen electrode (RHE; all the potentials in this report are versus RHE), low Tafel slope of 60−80 mV·decade^{-1} and high exchange current density of 3.0×10^{-5} A·cm^{-2}.

Cu_2O starting electrode was electrodeposited onto molybdenum coated glass slide employing a copper lactate bath.[26] Molybdenum substrate was preferred to the readily available fluorine-doped tin oxide (FTO) because the Cu_2O/Mo electrode showed enhanced mechanical stability compared with a Cu_2O/FTO counterpart from which Cu_2O layer is

Received: March 15, 2015
Revised: May 27, 2015
Published: June 1, 2015

DOI: 10.1021/acscatal.5b00556
ACS Catal. 2015, 5, 4115−4120

detached during electrochemical measurements at high current densities. Typically, the compact Cu_2O film of 1.5−3.0 μm thickness was grown. The Cu_2O electrode was then held at constant potential of +0.12 V vs RHE in a degassed pH 7 phosphate buffer solution (0.1 M) and illuminated for 10 min with 1 sun (Figure 1). The applied potential vs RHE was

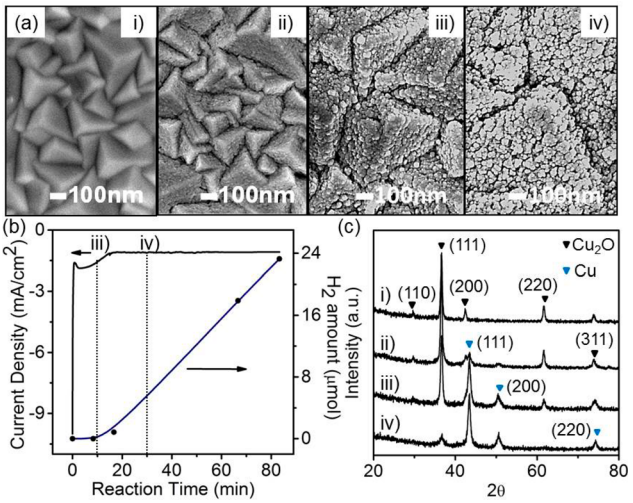

Figure 1. Cu/Cu_2O electrode characterizations. (a) Morphology evolution from Cu_2O electrode to final Cu/Cu_2O electrode during the photoelectrochemical (*hv*) and following electrochemical (dark) reduction process. (b) Evolution of current and H_2 yield (sum in headspace and solution) during electrochemical equilibration of Cu/Cu_2O electrode at −0.26 V vs RHE in a pH 7 phosphate buffer. The detailed calculation of dissolved H_2 in solution using Henry's law is shown in Figure S3. (c) XRD probing on Cu_2O electrode during the photoelectrochemical and electrochemical reduction process, corresponding to morphology evolution in part a. (i) Cu_2O; (ii) +0.12 V, *hv*, 10 min; (iii) −0.26 V, dark, 10 min; (iv) −0.26 V, dark, 30 min.

calibrated by HER/HOR (hydrogen evolution/oxidation reactions) on a Pt disk electrode in the hydrogen saturated electrolyte (Figure S1). After this exposure, the electrode was found to be no longer photoactive because of the formation of Cu/Cu_2O, which was previously explained as a Cu_2O-to-Cu corrosion process inhibiting the photoresponse of Cu_2O.[27,28] It was then further equilibrated at −0.26 V vs RHE in O2-free phosphate solution for 30 min to achieve steady cathodic current.

Scanning electron microscopy (SEM) showed the evolution of the morphology of Cu_2O electrode during the photoelectrochemical reduction process: from a compact structure which consisted of large grains to highly porous morphology made of small nanoparticles (Figure 1a). Corresponding sequential cross-section images are provided in Figure S2. Apparently, the electrochemical preparation resulted in an increase of specific surface area of Cu_2O electrode. X-ray diffraction was used to probe the reduction of Cu_2O into Cu during the preparation process (Figure 1c). As seen, the Cu_2O peaks decrease while those of Cu increase when the photoelectrochemical reduction process is prolonged. Remarkably, Cu_2O still remains when the steady-state electrode, showing steady catalytic current at −0.26 V vs RHE, was achieved. This steady-state was confirmed by XRD test for an electrode after 2 h electrolysis (Figure S4). Thus, we denote the as-prepared steady electrode (iv) as Cu/Cu_2O. We note that this Cu/Cu_2O electrode can be also obtained just by equilibrating a freshly prepared Cu_2O electrode in a pH 7 phosphate buffer solution at constant potential of −0.26 V vs RHE for a time period longer than 1 h. However, the Cu/Cu_2O electrode obtained through photoelectrochemical reduction exhibited higher stability.

Interestingly, during the equilibration at −0.26 V vs RHE, H_2 bubbles appeared on the electrode surface. Checking the amount of generated H_2 with time showed a negligible current-to-H_2 yield (detailed calculation method is given in the Supporting Information) of less than 1% for the first 500 s of bulk electrolysis. During this time the current is high but rapidly decreased (Figure 1b). Thus, the current passed through electrode is mainly due to the reduction of Cu_2O to Cu. However, with the increasing of Cu content, the catalytic HER was accelerated. When the Cu/Cu_2O electrode reached steady state, H_2 was produced with a current-to-H_2 yield close to unity and a Faradaic efficiency of 98% during 2000 s (~33 min) electrolysis at −0.26 V vs RHE. To exclude the influence of molybdenum substrate on Cu/Cu_2O electrode, polarization curves were measured under the same experiment conditions (see Figure S5a). The possibility of CuMo alloy formation can be excluded based on XRD analysis and EDS mapping on the electrode after 2 h electrolysis (Figure S4). The electrode exhibited a stable performance and the catalytic activity remained unchanged for more than 4 h (Figure S5b). Carbon paper was also used as substrate to fabricate the Cu/Cu_2O electrode. The film exhibited similar performance as shown in

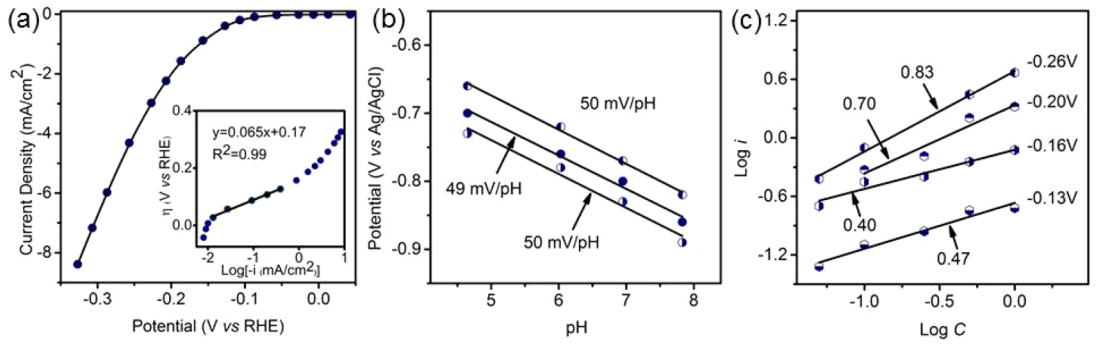

Figure 2. HER catalytic activities of the Cu/Cu_2O electrode in phosphate solution. (a) Catalytic currents versus applied potentials. (inset) Tafel plot. The steady currents were recorded by 15 min electrolysis at each applied potential step. (b) Plotting of potentials required as a function of electrolyte pHs to sustain constant catalytic currents j_{cat} of 0.2, 0.6, or 1.2 mA·cm^{-2}. (c) Catalytic activities (j_{cat}) recorded at overpotential of 130, 160, 200, and 260 mV as a function of phosphate concentration.

DOI: 10.1021/acscatal.5b00556
ACS Catal. 2015, 5, 4115−4120

Table 1. Activities of Non-Pt Electrocatalysts for HER

catalyst	electrolyte	onset potential [mV][a]	Tafel slope [mV·decade^{-1}]	refs
Cu/Cu_2O	0.5 M KPi (pH 7)	−30	65	this work
Cu	acid/alkaline	−(300−400)	200−300	20, 21, 30, 31
MoS_2	0.5 M H_2SO_4	−120	50	32
MoB and MoC_2	1.0 M H_2SO_4	−100	54−59	33
NiMoN/C	0.1 M $HClO_4$	−78	36	29
WS_2	0.5 M H_2SO_4	−100	48	34
NiP/Ti	0.5 M H_2SO_4	∼−50	46	35
CoP/Ti	0.5 M H_2SO_4	∼−40	50	36
CoP/CNT	0.5 M H_2SO_4	−40	54	37
$CoSe_2$/CF	0.5 M H_2SO_4	∼−100	40	38
$MoS_{2.7}$@NPG	0.2 M KPi (pH 7)	−120	60	39
Co−S/FTO	1.0 M KPi (pH 7)	−43	93	40
Cu_2MoS_4	0.1 M KPi (pH 7)/0.5 M H_2SO_4	−135	95	41

[a]Onset potential: the potential at which the hydrogen evolution occurred measured versus RHE, calculated according to ref 29.

Figure S6. However, during the electrolysis, the film detached and cracked, indicating a weak attachment of Cu/Cu_2O film on carbon paper.

The above results indicated Cu/Cu_2O electrode to be a promising electrocatalyst for HER in aqueous media at neutral pH. Consequently, we assayed in detail its catalytic activities in pH 7 phosphate buffer solution (0.5 M KPi). To do so, bulk electrolysis was carried out at different constant cathodic potentials until steady currents were achieved. The potential increment was 20−30 mV per experimental point. Current−voltage (I−V) characteristic curves and the corresponding log j versus overpotential η curves are presented in Figure 2a. Remarkably, a very low overpotential η of ca. 30 mV was determined following the method described by Chen et al.[29] In order to confirm the capability to catalyze H_2 generation at very low overpotentials, bulk electrolysis was carried out at constant potential of −0.055 V vs RHE for 5 h. Stable catalytic current was obtained and H_2 could be produced with current yield close to unity (Figure S7). Within the overpotential range from 30 to 130 mV, the Tafel slope was determined to be 65 mV·decade^{-1}, suggesting the fast kinetics for HER. Higher slope values of ca. 200 mV·decade^{-1} were found at higher overpotentials ($\eta \geq 180$ mV), presumably because of the mass transport limitation of proton substrate. The geometric exchange current density j_0 was determined to be 3.0×10^{-5} A·cm^{-2}. Thus, the current Cu/Cu_2O represents one of the best Pt-free electrocatalysts for the hydrogen generation measured in aqueous media (Table 1). As shown in Table 1, our catalyst is among the most active non-Pt electrocatalysts at neutral pH, which is a more practical condition for water electrolysis. Compared with Pt, to achieve a current density of 1 mA/cm$^2_{geo}$, Cu/Cu_2O electrode requires about 90 mV more overpotential than Pt (Figure S8). We also normalized the current density by the real electrochemical surface area (ESA) of the electrode (Figure S9−11), which confirm that the excellent performance of our copper-based electrode is not due to the high surface area.

We suggest that the presence of phosphate anions are most likely acting as proton transport mediators and that this is the key factor contributing to the unprecedented activities of our copper catalyst. We therefore investigated how the phosphate electrolyte concentration impacts on the performance of the Cu/Cu_2O catalyst. To do so, steady catalytic currents were measured on the same Cu/Cu_2O electrode in electrolyte with different phosphate concentrations, buffered at pH 7. At low overpotentials (η = 130−160 mV), slopes of 0.4−0.5 were determined from the log j_{cat} versus log C (phosphate concentration) plot (Figure 2c). Increased slopes of ∼0.8 were determined at higher overpotential of 260 mV. These results are consistent with the increase of Tafel slope when overpotentials are increased to higher values (Figure 2a). In other words, at high overpotentials, the kinetic of HER on Cu/Cu_2O catalyst is fast and therefore the reaction rate is limited by the mass transport of protons to the catalytic sites. This in turn is dependent on the availability of phosphate anions. However, the involvement of phosphate anions at low overpotentials when the H_2 generation rate is slow is unexpected. Moreover, at low catalytic currents (j_{cat} 0.2, 0.6, or 1.2 mA·cm^{-2}), pH titration shows a dependence of ca. 50 mV·pH^{-1} (Figure 2b), indicating the H_2 evolution is limited by a $1e^-$, $1H^+$ electrochemical process. Therefore, it seems that the involvement of phosphate anions contributes to efficiency of transferring protons to vicinity of the catalytic sites on electrode surface.

We assume there is equilibrium between phosphate anions in the bulk solution and those chemically adsorbed on Cu/Cu_2O electrode surface. To investigate the impact of adsorbed phosphate anions, we carried out potential polarization studies on Cu/Cu_2O electrode in pH 6.9 Na_2SO_4 (0.1 M) solution free of any phosphate anions. We found that the catalytic activities are significantly lower than those observed in phosphate solution. As shown in curves P-S-1 to P-S-5 in Figure 3, HER occurred at overpotential of ∼180 mV while in phosphate buffer an overpotential of only 30 mV is required (Figure 2a). Prior to the HER catalytic event, we observed two reduction peaks at −0.055 and −0.15 V, assigned to electrochemical desorption of adsorbed phosphate anion from Cu/Cu_2O surface.[42] This desorption is completed once potential is polarized to −0.45 V and is accompanied by a drastically decrease of catalytic activity (P-S-5). This electrode now display similar activity compared to the electrode counterpart prepared in a sulfate solution (S-S-1). We also note that the morphology of this copper-based electrode is unchanged when prepared in different electrolyte solution with or without phosphate, e.g. SO_4^{2-}, ClO_4^-, halide (Figure S12−S14). Therefore, we conclude that the phosphate anions contribute to enhance catalytic activity of the Cu/Cu_2O catalyst rather than the high specific surface area caused by the mesoporous structure, a factor important for conventional crystalline copper electrodes. The adsorption of phosphate anions on Cu/Cu_2O electrode

DOI: 10.1021/acscatal.5b00556
ACS Catal. 2015, 5, 4115−4120

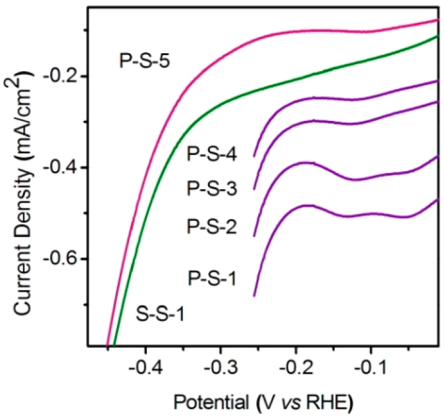

Figure 3. HER activities of Cu/Cu_2O electrode in phosphate-free solution. (P-S-1 to P-S-4) Four consecutive potential polarizations on Cu/Cu_2O electrode in pH 6.9 Na_2SO_4 (0.1 M) solution. (P-S-5) Potential polarization to more negative potential. (S-S-1) Polarization curve obtained in the same Na_2SO_4 solution employing a control Cu/Cu_2O electrode which was prepared following the electrochemical reduction process described but in Na_2SO_4 solution instead of phosphate solution.

was also confirmed by energy dispersive X-ray spectroscopy (EDS) mapping (Figure 4). In contrast, no phosphorus exists on the electrode surface when treated in phosphate-free electrolyte solution e.g. SO_4^{2-} (Figure S15).

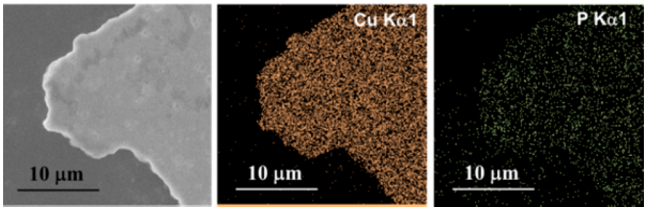

Figure 4. SEM and EDS mapping images of Cu/Cu_2O electrode after treatment in pH 7 phosphate buffer (0.1 M) solution.

It is known that phosphate and carbonate/carboxylate ions are chosen in nature to construct proton transfer networks.[43,44] Furthermore, carbonate and phosphate display similar chemical adsorption properties on electrode surfaces composed of crystalline Cu(111).[45] Therefore, it is interesting to investigate the catalytic activities of the Cu/Cu_2O electrode in a carbonate buffer solution. Indeed, we found that in a CO_2-saturated $NaHCO_3$ (0.5 M) solution at pH 7.4, the Cu/Cu_2O electrode displayed comparable catalytic currents to those obtained at same overpotentials in phosphate electrolyte (Figure S16). The onset potential η and Tafel slope value were determined to be ~50 mV and 80 mV·decade^{-1}, respectively. The catalytic current was also dependent on the concentration of carbonate anions (Figure S17). Bulk electrolysis carried out at both low (η = 240 mV) and higher (η = 540 mV) overpotentials showed current-to-H_2 yields close to unity. Neither CO nor formate were found as products (refers to the SI for details). This finding contrasts to those reported by Qiao et al.[46] and Li and Kanan[47] who showed high selective CO_2-to-CO reduction employing nanostructured copper electrodes. The obvious difference between our current copper electrode and those reported is the remaining of the Cu_2O phase. This oxide phase acts as anchoring sites for the chemical absorption of phosphate/carbonate ligand producing Cu^I-O-PO_3 or Cu^I-O-CO_3 species which serves as actual catalytic active sites for the proton reduction reaction. The possible adsorption state of the species could be derived from FT-IR spectroscopy (Figure 5a).

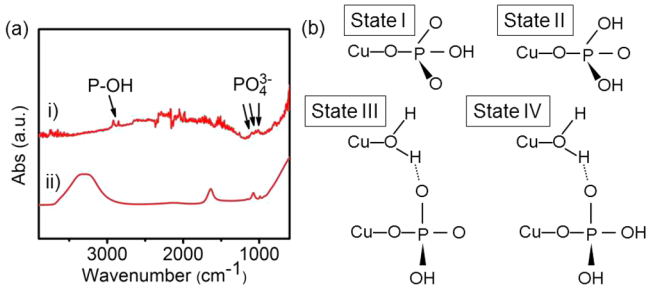

Figure 5. (a) FTIR spectra of (i) the Cu/Cu_2O activated in phosphate pH = 7 and (ii) free phosphate buffer solution pH = 7. Peaks at approximately 1300−2500 and 3400−3900 cm^{-1} are due to atmospheric H_2O/CO_2. (b) Several possible molecular geometries for the monodentate complex of Cu and phosphate species according to refs 48 and 49: state I-monoprotonated monodentate mononuclear; state II-deprotonated monodentate mononuclear; state III-monoprotonated monodentate mononuclear with H-bonded to surface water; state IV-deprotonated monodentate mononuclear with H-bonded to surface water.

A broad peak (PO_4^{3-}) comprised of overlapping bands corresponding to frequencies of 1096, 1048, and 1004 cm^{-1} was observed for the phosphate on Cu/Cu_2O electrode. Compared with free phosphate, the splitting pattern and the frequencies of the adsorption bands indicate a monodentate surface complex with lower symmetry upon adsorption, as shown in Figure 5b.[48−51]

Employing the Cu/Cu_2O electrode, we achieved catalytic CO_2 reduction activities from a CO_2-saturated DMF solution containing 1% water. Products analysis carried on the basis of 1 h electrolysis at −1.5 V vs Ag/AgCl showed production of HCOOH (64%), CO (6.2%), and H_2 (4.5%). This result together with those of selective H_2 production from aqueous carbonate buffer solutions suggest that the catalytic reaction was initiated by reduction of protons providing hydride intermediates, type $[Cu^{II}–H^-]^+$.[52] Thus, we propose mechanistic pathways for the reduction reactions centered on Cu^I–L catalytic centers where L is chemically adsorbed phosphate or carbonate ligands (eqs 1−5). The formation of hydride intermediates via the $1e^-$, $1H^+$ electrochemical reduction process of protonated Cu^I–LH^+ species (eq 2) is believed to be rate-limiting step. This is supported by a dependence of ca. 50 mV per pH was determined for external applied bias to sustain a constant catalytic current in different pH solutions (Figure 2b). The hydride intermediate species lead subsequently to electrophilic attack of CO_2 molecules resulting in production of formate (eq 4). Alternatively when the proton activities of the medium are high e.g. within carbonate buffer, the protonation of the hydride intermediates is favored (eq 3), which hinders the CO_2 reduction.

$$Cu^I–L + H^+ \leftrightarrow Cu^I–LH^+ \quad (1)$$

$$Cu^I–LH^+ + 1e^- + 1H^+ \rightarrow (Cu^{II}–H^-)–LH^+ \quad (2)$$

$$(Cu^{II}–H^-)–LH^+ \rightarrow Cu^{II}–L + H_2 \quad (3)$$

Or

DOI: 10.1021/acscatal.5b00556
ACS Catal. 2015, 5, 4115−4120

$$(Cu^{II}–H^{-})–LH^{+} + CO_2 \rightarrow (Cu^{II}–HCO_2)–LH^{+} \rightarrow Cu^{II}–L + HCOOH \quad (4)$$

$$Cu^{II}–L + 1e^{-} \rightarrow Cu^{I}–L \quad (5)$$

In summary, we report here a (photo)electrochemical approach to activate the copper-based electrode for high efficient hydrogen evolution from water. We show for the first time that a copper-based electrocatalyst, Cu/Cu_2O, can selectively generate H2 in an aqueous environment at neutral or near-to-neutral pH with a small over potential requirement. Chemically adsorbed phosphate plays an important role in accelerating the catalytic hydrogen evolution rate on the Cu/Cu_2O catalyst surface. This catalyst represents an attractive alternative to Pt for HER.

■ ASSOCIATED CONTENT

Supporting Information

The Supporting Information is available free of charge on the ACS Publications website at DOI: 10.1021/acscatal.5b00556.

Experiment details, calculation of Faradaic efficiency, and real electrochemical surface area, additional characterization data, and figures including SEM images and bulk electrolysis (PDF)

■ AUTHOR INFORMATION

Corresponding Authors

*E-mail: xuzc@ntu.edu.sg (Z.J.X.).
*E-mail: dptran@ntu.edu.sg (P.D.T.).
*E-mail: joachimLoo@ntu.edu.sg (J.S.C.L.).

Notes

The authors declare no competing financial interest.

■ ACKNOWLEDGMENTS

J.Z. thanks Energy Research Institute @ Nanyang Technological University (ERI@N) and the Singapore–Berkeley Research Initiative for Sustainable Energy (SinBeRISE) CREATE for postdoctoral fellowship. J.Z., P.D.T., J.S.C.L., Z.J.X. and J.B. acknowledge the Centre for Artificial Photosynthesis (CAP-NTU) and the SinBeRISE CREATE for financial and facilities supports.

■ REFERENCES

(1) Tran, P. D.; Wong, L. H.; Barber, J.; Loo, J. S. C. *Energy Environ. Sci.* **2012**, *5*, 5902–5918.
(2) Barber, J.; Tran, P. D. *J. R. Soc., Interface* **2013**, *10*, 0984.
(3) Hu, S.; Xiang, C.; Haussener, S.; Berger, A. D.; Lewis, N. S. *Energy Environ. Sci.* **2013**, *6*, 2984–2993.
(4) Walter, M. G.; Warren, E. L.; McKone, J. R.; Boettcher, S. W.; Mi, Q. X.; Santori, E. A.; Lewis, N. S. *Chem. Rev.* **2010**, *110*, 6446–6473.
(5) DuBois, D. L. *Inorg. Chem.* **2014**, *53*, 3935–3960.
(6) Jacques, P. A.; Artero, V.; Pecaut, J.; Fontecave, M. *Proc. Natl. Acad. Sci. U. S. A.* **2009**, *106*, 20627–20632.
(7) Artero, V.; Kerlidou, M. C.; Fontecave, M. *Angew. Chem., Int. Ed.* **2011**, *50*, 7238–7266.
(8) Tran, P. D.; Goff, A. L.; Heidkamp, J.; Jousselme, B.; Guillet, N.; Palacin, S.; Dau, H.; Fontecave, M.; Artero, V. *Angew. Chem., Int. Ed.* **2011**, *50*, 1371–1374.
(9) Tard, C.; Pickett, C. J. *Chem. Rev.* **2009**, *109*, 2245–2274.
(10) Gloaguen, F.; Rauchfuss, T. B. *Chem. Soc. Rev.* **2009**, *38*, 100–108.
(11) Cobo, S.; Heidkamp, J.; Jacques, P. A.; Fize, J.; Fourmond, V.; Guetaz, L.; Jousselme, B.; Ivanova, V.; Dau, H.; Palacin, S.; Fontecave, M.; Artero, V. *Nat. Mater.* **2012**, *11*, 802–807.
(12) He, C.; Wu, X.; He, Z. *J. Phys. Chem. C* **2014**, *118*, 4578–4584.
(13) Kanan, M. W.; Nocera, D. G. *Science* **2008**, *321*, 1072–1075.
(14) Dincă, M.; Surendranath, Y.; Nocera, D. G. *Proc. Natl. Acad. Sci. U. S. A.* **2010**, *107*, 10337–10341.
(15) Joya, K. S.; Takanabe, K.; Groot, H. J. M. *Adv. Energy Mater.* **2014**, *4*, 1400252.
(16) Barnett, S. M.; Goldberg, K. I.; Mayer, J. M. *Nat. Chem.* **2012**, *4*, 498–502.
(17) Zhang, T.; Wang, C.; Liu, S.; Wang, J. L.; Lin, W. *J. Am. Chem. Soc.* **2014**, *136*, 273–281.
(18) Chen, Z.; Meyer, T. J. *Angew. Chem., Int. Ed.* **2013**, *52*, 700–703.
(19) Zhang, M.; Chen, Z.; Kang, P.; Meyer, T. J. *J. Am. Chem. Soc.* **2013**, *135*, 2048–2051.
(20) Brisard, G.; Bertrand, N.; Ross, P. N.; Marković, N. M. *J. Electroanal. Chem.* **2000**, *480*, 219–224.
(21) Sheng, W.; Myint, M.; Chen, J. G.; Yan, Y. *Energy Environ. Sci.* **2013**, *6*, 1509–1512.
(22) Kumar, B.; Saha, S.; Ganguly, A.; Ganguli, A. K. *RSC Adv.* **2014**, *4*, 12043–12049.
(23) Kumar, B.; Saha, S.; Basu, M.; Ganguli, A. K. *J. Mater. Chem. A* **2013**, *1*, 4728–4735.
(24) Kumar, B.; Saha, S.; Ojha, K.; Ganguli, A. K. *Mater. Res. Bull.* **2015**, *64*, 283–287.
(25) Zhang, P. L.; Wang, M.; Yang, Y.; Yao, T. Y.; Sun, L. C. *Angew. Chem., Int. Ed.* **2014**, *53*, 13803–13807.
(26) Chen, Y.; Tran, P. D.; Boix, P. P.; Bassi, P. S.; Yantara, N.; Wong, L. H.; Barber, J. *Nanoscale* **2014**, *6*, 6506–6510.
(27) Li, C. L.; Li, Y. B.; Delaunay, J. J. *ACS Appl. Mater. Interfaces* **2014**, *6*, 480–486.
(28) Paracchino, A.; Brauer, J. C.; Moser, J. E.; Thimsen, E.; Grätzel, M. *J. Phys. Chem. C* **2012**, *116*, 7341–7350.
(29) Chen, W. F.; Sasaki, K.; Ma, C.; Frenkel, A. I.; Marinkovic, N.; Muckerman, J. T.; Zhu, Y. M.; Adzic, R. R. *Angew. Chem., Int. Ed.* **2012**, *51*, 6131–6135.
(30) Bockris, J. O'M.; Pentland, N. *Trans. Faraday Soc.* **1952**, *48*, 833–839.
(31) Björketun, M. E.; Bondarenko, A. S.; Abrams, B. L.; Chorkendorff, I.; Rossmeisl, J. *Phys. Chem. Chem. Phys.* **2010**, *12*, 10536–10541.
(32) Xie, J. F.; Zhang, H.; Li, S.; Wang, R. X.; Sun, X.; Zhou, M.; Zhou, J. F.; Lou, X. W.; Xie, Y. *Adv. Mater.* **2013**, *25*, 5807–5813.
(33) Vrubel, H.; Hu, X. *Angew. Chem., Int. Ed.* **2012**, *51*, 12703–12706.
(34) Cheng, L.; Huang, W. J.; Gong, Q. F.; Liu, C. H.; Liu, Z.; Li, Y. G.; Dai, H. J. *Angew. Chem., Int. Ed.* **2014**, *53*, 7860–7863.
(35) Popczun, E. J.; McKone, J. R.; Read, C. G.; Biacchi, A. J.; Wiltrout, A. M.; Lewis, N. S.; Schaak, R. E. *J. Am. Chem. Soc.* **2013**, *135*, 9267–9270.
(36) Popczun, E. J.; Read, C. G.; Roske, C. W.; Lewis, N. S.; Schaak, R. E. *Angew. Chem., Int. Ed.* **2014**, *53*, 5427–5230.
(37) Liu, Q.; Tian, J. Q.; Cui, W.; Jiang, P.; Cheng, N. Y.; Asiri, A. M.; Sun, X. P. *Angew. Chem.* **2014**, *53*, 6828–6832.
(38) Kong, D.; Wang, H.; Lu, Z.; Cui, Yi. *J. Am. Chem. Soc.* **2014**, *36*, 4897–4900.
(39) Ge, X. B.; Chen, L. Y.; Zhang, L.; Wen, Y. R.; Hirata, A.; Chen, M. W. *Adv. Mater.* **2014**, *26*, 3100–3104.
(40) Sun, Y. J.; Liu, C.; Grauer, D. C.; Yano, J.; Long, J. R.; Yang, P. D.; Chang, C. J. *J. Am. Chem. Soc.* **2013**, *135*, 17699–17702.
(41) Tran, P. D.; Nguyen, M.; Pramana, S. S.; Bhattacharjee, A.; Chiam, S. Y.; Fize, J.; Field, M. J.; Artero, V.; Wong, L. H.; Loo, J.; Barber, J. *Energy Environ. Sci.* **2012**, *5*, 8912–8916.
(42) Schlaup, C.; Horch, S. *Surf. Sci.* **2013**, *608*, 44–54.
(43) Burget, U.; Zundel, G. *Biopolymers* **1987**, *26*, 95–108.
(44) Jalbout, A. F.; Zhang, L. Q.; Li, H. R.; Hu, X. B. *Chem. Phys. Lett.* **2007**, *446*, 25–30.
(45) Magnussen, O. M. *Chem. Rev.* **2002**, *102*, 679–726.

DOI: 10.1021/acscatal.5b00556
ACS Catal. 2015, 5, 4115–4120

(46) Qiao, J. L.; Jiang, P.; Liu, J. S.; Zhang, J. J. *Electrochem. Commun.* **2014**, *38*, 8−11.
(47) Li, C. W.; Kanan, M. W. *J. Am. Chem. Soc.* **2012**, *134*, 7231−7234.
(48) Rubasinghege, G.; Kyei, P. K.; Scherer, M. M.; Grassian, V. H. *J. Colloid Interface Sci.* **2012**, *385*, 15−23.
(49) Mudunkotuwa, I. A.; Minshid, A. A.; Grassian, V. H. *Analyst* **2014**, *139*, 870−881.
(50) Martens, W.; Frost, R. L. *Am. Mineral.* **2003**, *88*, 37−46.
(51) Stoch, A.; Jastrzębski, W.; Brożek, A.; Stoch, J.; Szaraniec, J.; Trybalska, B.; Kmita, G. *J. Mol. Struct.* **2000**, *555*, 375−382.
(52) Halpern, J.; Macgregor, E. R.; Peters, E. *J. Phys. Chem.* **1956**, *60*, 1455−1456.

DOI: 10.1021/acscatal.5b00556
ACS Catal. 2015, 5, 4115−4120